Magnetic properties of a spin-$\frac{1}{2}$ honeycomb lattice antiferromagnet

Y. Kono,[1,*] T. Okabe,[1] N. Uemoto,[1] Y. Iwasaki,[1] Y. Hosokoshi,[1] S. Kittaka,[2] T. Sakakibara,[2] and H. Yamaguchi[1,†]

[1]*Department of Physical Science, Osaka Prefecture University, Osaka 599-8531, Japan*

[2]*Institute for Solid State Physics, the University of Tokyo, Chiba 277-8581, Japan*

(Received 8 September 2019; revised manuscript received 7 January 2020; published 24 January 2020)

We present an $S = 1/2$ antiferromagnetic (AF) honeycomb lattice composed of a verdazyl-based complex $[Zn(hfac)_2][o\text{-Py-V-(4-F)}_2]$. *Ab initio* molecular orbital calculations indicate that two AF interactions and a ferromagnetic interaction lead to the formation of a honeycomb lattice. We explain the magnetic susceptibility, magnetization curve, and magnetic specific heat based on the $S = 1/2$ Heisenberg AF honeycomb lattice using the quantum Monte Carlo method. Further, by considering the distortion effect on the magnetic behavior, we confirm that the dimer-like lattice distortion in the present compound is small enough not to affect the intrinsic two-dimensional properties of the honeycomb lattice. Our numerical study on the distorted honeycomb lattice reveals a quantum phase transition from a disordered dimer phase to an AF ordered phase at a critical distortion ratio.

DOI: 10.1103/PhysRevB.101.014437

I. INTRODUCTION

Two-dimensional (2D) $S = 1/2$ Heisenberg antiferromagnetic (HAF) spin systems have received considerable attention as parent insulating states of high-temperature superconductors in layered cuprates. The most studied example is the $S = 1/2$ HAF square lattice. Although it exhibits a long-range Néel order in its ground state, the effect of quantum fluctuations reduces the magnetic moment per site by approximately 40% with respect to its conventional value [1]. The $S = 1/2$ HAF honeycomb lattice is another intriguing 2D bipartite spin system. Recent studies on graphene [2,3] and an exactly solvable Kitaev model with strong anisotropic interactions [4] have garnered further interest in honeycomb lattices. Although the $S = 1/2$ HAF honeycomb lattice exhibits a Néel order in its ground state, the quantum fluctuations are enhanced because of its low 2D coordination number. This further reduces the magnetic moment per site relative to that of the square lattice [5–9] and makes its ordered state fragile. Numerical investigations on a distorted honeycomb lattice revealed that relatively small lattice distortions can destroy the ordered state and induce a disordered phase [10–12]. The dimer-like distortion, which is similar to the distortion in the present model, causes a quantum phase transition (QPT) from the AF ordered phase to a gapped dimer phase at a critical distortion ratio. The evaluated quantum critical exponents indicate that the quantum criticality falls in the $O(3)$ universality class.

From an experimental viewpoint, among inorganic compounds, there are only a few model substances for the $S = 1/2$ HAF honeycomb lattice [13–15]. Copper oxide $InCu_{2/3}V_{1/3}O_3$ is known as a candidate with an equivalent exchange interaction of $J/k_B = 280$ K [13,16–18]. However, structural domains of approximately 300 Å exist in a 2D hexagonal plane [16]. Therefore, it is unclear whether the magnetic behavior in the case of $InCu_{2/3}V_{1/3}O_3$ originates from intrinsic quantum nature or the finite-size effect in the domain boundaries. Copper coordination polymer $Cu_2(pymca)_3(ClO_4)$ with an exchange interaction $J/k_B = 37$ K is another candidate for the equivalent model [15]. The β modification of $Cu_2V_2O_7$ is expected to form a slightly distorted lattice with an averaged exchange interaction $J/k_B = 60$–66 K, and a phase transition to the long-range Néel order is observed at 26 K [14]. Considering the energy scale of the exchange interactions in the above inorganic compounds, it is difficult to examine the quantum behavior of the $S = 1/2$ HAF honeycomb lattice in magnetic fields up to the saturation field. Conversely, organic compounds have relatively weak exchange interactions owing to their intermolecular couplings. Verdazyl radicals, which have been developed for quantum spin systems, can form several $S = 1/2$ distorted HAF honeycomb lattices [19–21]. In verdazyl radical 2-Cl-3,6-F_2-V [=3-(2-chloro-3,6- difluorophenyl)-1,5-diphenylverdazyl] and 2-Cl-6-F-V [= 3-(2-chloro-6-fluorophenyl)-1,5- diphenylverdazyl], uniform AF chains connected by slightly weak AF interactions and uniform ferromagnetic chains connected by AF interactions are formed, respectively. The magnetic behaviors in the case of verdazyl compounds have been observed up to the saturation field and quantitatively described using honeycomb lattice models [19,20].

In this paper, we present a verdazyl-based complex forming an $S = 1/2$ HAF honeycomb lattice. We synthesized single crystals of $[Zn(hfac)_2][o\text{-Py-V-(4-F)}_2]$ [hfac = 1,1,1,5,5,5-hexafluoroacetylacetonate, o-Py-V-(4-F)$_2$ = 3-(2-pyridyl)-1,5-bis(4-fluorophenyl)-diphenylverdazyl]. *Ab initio* molecular orbital (MO) calculations indicated that three types of predominant interactions lead to the formation of an $S = 1/2$ honeycomb lattice. We explained the magnetic susceptibility, magnetization curve, and magnetic specific heat based on the $S = 1/2$ HAF honeycomb lattice using the quantum Monte Carlo (QMC) method. Further, we examined the effects of lattice distortion on the magnetic behavior and found a critical distortion ratio at which a QPT occurs from a disordered dimer phase to an AF ordered phase.

*y.kono@p.s.osakafu-u.ac.jp
†yamaguchi@p.s.osakafu-u.ac.jp

II. EXPERIMENTAL AND NUMERICAL METHOD

We synthesized *o*-Py-V-(4-F)$_2$ through a conventional procedure for verdazyl radical [22]. A solution of [Zn(hfac)$_2$] · 2H$_2$O (51.5 mg, 0.1 mmol) in 15 ml of heptane was refluxed at 70° C. A solution of *o*-Py-V-(4-F)$_2$ (35.0 mg, 0.1 mmol) in 2 ml of CH_2Cl_2 was slowly added, and stirring was continued for 1 h. After the mixed solution cooled to room temperature, a dark-green crystalline solid of [Zn(hfac)$_2$][*o*-Py-V-(4-F)$_2$] was separated by filtration and washed with heptane. The dark-green residue was recrystallized using acetonitrile at 10° C.

A single-crystal x-ray diffraction (XRD) experiment was performed by using a Rigaku AFC-8R Mercury CCD RAMicro7 diffractometer with Japan Thermal Engineering XRHR10K. The single crystal XRD data are refined by using the SHELX software [23]. The structural refinement was carried out using anisotropic and isotropic thermal parameters for the nonhydrogen atoms and the hydrogen atoms, respectively. Restrains or constrains were used for atomic hydrogen positions and thermal displacements.

The magnetic susceptibility was measured using a commercial superconducting quantum interference device (SQUID) magnetometer (MPMS-XL, Quantum Design) with a ^{3}He refrigerator down to about 0.5 K. The magnetization curve was measured using a capacitive Faraday magnetometer with a dilution refrigerator at 0.1 K. The experimental results were corrected for the diamagnetic contribution of -5.1×10^{-4} emu mol^{-1}, which is determined to become almost $\chi^{-1} \propto T$ above approximately 10 K and close to that calculated by Pascal's method. The specific heat was measured with a commercial calorimeter (PPMS, Quantum Design) using a thermal relaxation method above 1.9 K and a handmade apparatus by a standard adiabatic heat-pulse method with a ^{3}He refrigerator down to about 0.3 K. There is no significant difference in magnetic properties between the field directions owing to the isotropic g value of ∼2.004 in verdazyl radical systems [24,25]. Therefore, all experiments were performed using small randomly oriented single crystals.

Ab initio MO calculations were performed using the UB3LYP method with the basis set 6-31G in the GAUSSIAN09 program package. The convergence criterion was set at 10^{-8} hartree. For the estimation of intermolecular magnetic interaction, we applied our evaluation scheme that was studied previously [26].

The QMC code is based on the directed loop algorithm in the stochastic series expansion representation [27]. The calculations for the $S = 1/2$ HAF honeycomb lattice was performed for $N = 1152$ under the periodic boundary condition, where N denotes the system size. It was confirmed that there is no significant size-dependent effect. All calculations were carried out using the ALPS application [28,29].

III. RESULTS AND DISCUSSION

A. Crystal structure and magnetic model

The crystallographic data for the synthesized [Zn(hfac)$_2$][*o*-Py-V-(4-F)$_2$] are summarized in Table I, and the molecular structure is shown in Fig. 1(a). The verdazyl ring (which includes four N atoms), the upper two phenyl rings, and the bottom pyridine ring are labeled R$_1$, R$_2$, R$_3$, and R$_4$, respectively. The dihedral angles of R$_1$-R$_2$, R$_1$-R$_3$, R$_1$-R$_4$ are approximately 15°, 48°, and 8°, respectively. Each molecule has a delocalized $S = 1/2$ spin. The result of the MO calculation for the [Zn(hfac)$_2$][*o*-Py-V-(4-F)$_2$] molecule indicates that approximately 59% of the total spin density is present on R$_1$. Figure 1(b) shows the corresponding spin-density distribution. Further, while R$_2$ and R$_3$ each account for approximately 17% of the relatively large total spin density, R$_4$ accounts for less than 6% of the total spin density. Therefore, the intermolecular interactions are caused by the short contacts related to the R$_1$, R$_2$, and R$_3$ rings. Since Zn(hfac)$_2$ has a low spin density less than 1% of the total spin density, it works as a spacer between verdazyl radicals. We focus on the structural features related to the *o*-Py-V-(4-F)$_2$ to consider intermolecular interactions.

We evaluated the intermolecular exchange interactions of all molecular pairs within 4.0 Å through the *ab initio* MO calculations and found three types of predominant interactions. They are evaluated as $J_1/k_B = 7.4$ K, $J_2/k_B = 5.6$ K,

TABLE I. Crystallographic data for [Zn(hfac)$_2$][*o*-Py-V-(4-F)$_2$].

Formula	$C_{29}H_{16}F_{14}N_5O_4Zn$	
Crystal system	Monoclinic	
Space group	$P2_1/c$	
Temperature (K)	RT	25(2)
Wavelength (Å)	0.7107	
a(Å)	9.141(4)	8.898(2)
b(Å)	31.879(14)	31.491(9)
c(Å)	10.945(5)	10.859(3)
β (degrees)	92.170(5)	91.347(4)
V (Å^3)	3187(2)	3041.9(14)
Z	4	
D_{calc} (g cm^{-3})	1.729	1.812
Measured reflections	5590	5258
Reflection merged	4586	3380
Parameters refined	478	
$R\,[I > 2\sigma(I)]$	0.0636	0.0631
$R_w\,[I > 2\sigma(I)]$	0.1565	0.1525
Goodness of fit	1.077	0.945
CCDC	1 952 182	1 952 183

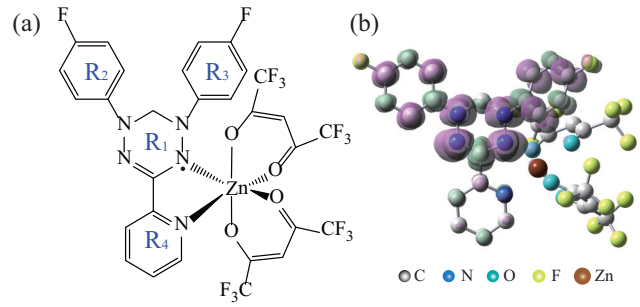

FIG. 1. (a) Molecular structure of [Zn(hfac)$_2$][*o*-Py-V-(4-F)$_2$] and (b) its spin-density distribution. Purple and green shapes correspond to positive and negative spin densities, respectively. The isodensity surface corresponds to a cutoff value of 0.001e bohr^{-3}.

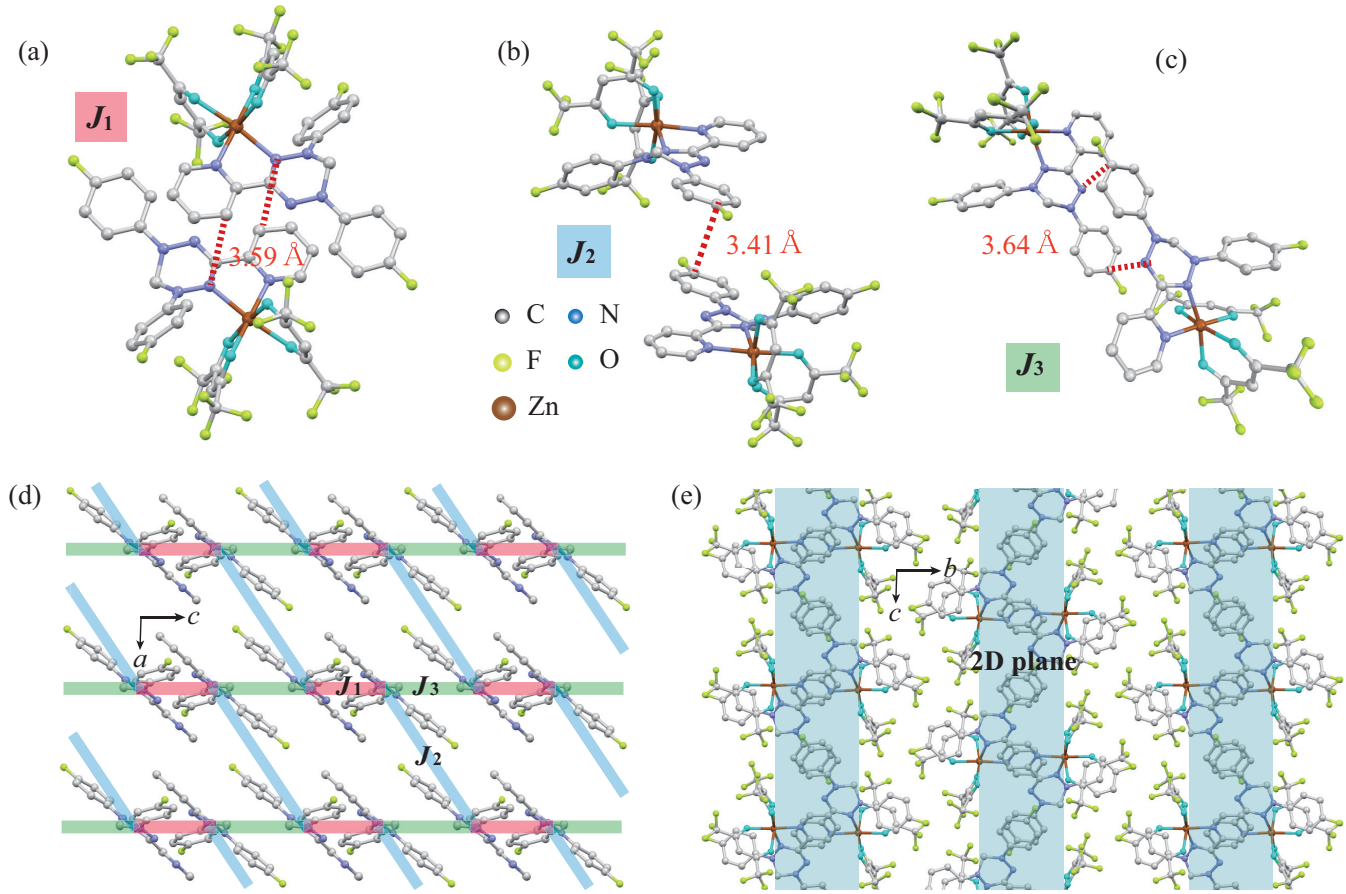

FIG. 2. Molecular pair of $[Zn(hfac)_2][o\text{-Py-V-(4-F)}_2]$ associated with the exchange interactions (a) J_1, (b) J_2, and (c) J_3. Hydrogen atoms are omitted for clarity. The broken lines indicate N-C and C-C short contacts. (d) Crystal structure forming a 2D honeycomb lattice in the *ac* plane, in which each $Zn(hfac)_2$ in the molecule is omitted for clarity. (e) Crystal structure viewed parallel to the 2D honeycomb plane.

and $J_3/k_B = -3.8$ K, which are defined in the Heisenberg spin Hamiltonian given by $\mathcal{H} = J_n \sum_{<i,j>} S_i \cdot S_j$, where $\sum_{<i,j>}$ denotes the sum over the neighboring spin pairs. All molecular pairs associated with these interactions are related by an inversion center, and the N-C and C-C short contacts for the J_1, J_2, and J_3 interactions are given by 3.59, 3.41, and 3.64 Å, respectively, as shown in Figs. 2(a) to 2(c). The three dominant interactions lead to the formation of an $S = 1/2$ honeycomb lattice in the *ac* plane, as shown in Fig. 2(d). Although the molecular arrangement is not hexagonal, the spin network is topologically equivalent to the honeycomb lattice considering the isotropic nature of organic radical systems. The nonmagnetic $Zn(hfac)_2$ acts as a spacer between the 2D structures, as shown in Fig. 2(e). The interplane couplings are evaluated to be less than approximately 1/50 of J_1 in absolute values.

B. Magnetic and thermodynamic properties

Figure 3(a) shows the temperature dependence of the magnetic susceptibility ($\chi = M/H$) at 0.1 T. Above 10 K, it follows the Curie-Weiss law, and the Curie constant and Weiss temperature are estimated to be 0.362 emu K/mol and $\theta_W = -1.2$ K, respectively. This small value of θ_W indicates contributions of both ferromagnetic and AF interactions as suggested by the MO calculations. We evaluated the paramagnetic impurities to be approximately 1.2% of all spins, which is defined to fit the following calculated result and is close to those evaluated in other verdazyl radical crystals [30,31], and subtracted it from the raw data by assuming conventional paramagnetic behavior. The corrected data in Fig. 3(a) are normalized by subtracting the impurities. We observe a broad peak at approximately 2.2 K, which indicates an AF short-range order in the honeycomb lattice. We calculated the magnetic susceptibility for the $S = 1/2$ HAF honeycomb lattice using the QMC method. Here, for simplicity, we assumed a uniform model with J_1=$J_2 = |J_3|$. Given the radical-based compound, we used the isotropic *g*-value of 2.00. We obtained a good agreement between the experimental and calculation results when $J_1/k_B = 3.6$ K with a radical purity of 95%, as shown in Fig. 3(a).

Figure 3(b) shows the magnetization curve at 0.1 K. The magnetization curve clearly indicates a combined behavior of a linear increase and Brillouin function in the low-field region. Thus, we can determine the amount of paramagnetic impurities and obtain an intrinsic behavior so that low-field increase becomes smooth. We subtracted a small paramagnetic contribution given by the Brillouin function in the low-field region that is evaluated to account for 4.3% of all spins. The corrected data in Fig. 3(b) is normalized by subtracting the impurities. These paramagnetic impurities are slightly larger

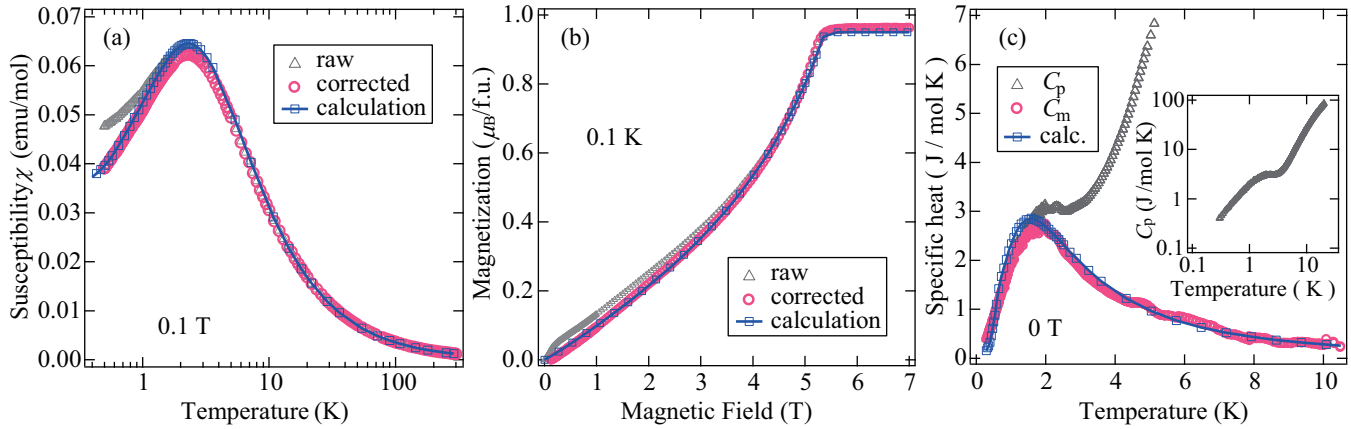

FIG. 3. Magnetic and thermodynamic properties of $[Zn(hfac)_2][o\text{-Py-V-(4-F)}_2]$. (a) Temperature dependence of magnetic susceptibility ($\chi = M/H$) at 0.1 T. The open triangles denote raw data, and the open circles are corrected for the paramagnetic term due to the impurity. (b) Magnetization curve at 0.1 K. The open triangles denote raw data, and the open circles are corrected for the paramagnetic term due to the impurity. (c) Total specific heat C_p and its magnetic contribution C_m at 0 T. The inset shows C_p up to 20 K. The solid lines with open squares represent the calculated results for the $S = 1/2$ uniform HAF honeycomb lattice with the relation of $J_1{=}J_2{=}|J_3|$ ($\alpha = 1.0$).

than those evaluated from the magnetic susceptibility. This difference is considered to originate from the measurement setting as well as the sample differences. For the measurement using capacitive Faraday magnetometer, we use grease to fix the sample on the capacitance stage. The paramagnetic contribution is considered to be increased by the radicals dissolve in the grease. We observe nonlinear behavior originating from quantum fluctuations in the $S = 1/2$ honeycomb lattice. We calculated the magnetization curve at 0.1 K assuming the same model as for the magnetic susceptibility by using the same parameters and obtained good agreement between the experiment and the calculation, as shown in Fig. 3(b).

The inset of Fig. 3(c) shows the experimental results of the total specific heat C_p at zero field. A clear shoulder is observed at approximately 2 K. We evaluated the magnetic specific heat C_m by subtracting the lattice contribution C_l and assumed C_l in the low-temperature region approximated as $C_l = a_1T^3 + a_2T^5 + a_3T^7$. The constants $a_1 - a_3$ are determined to reproduce the following magnetic specific heat calculated by the QMC method. As a result, C_l was evaluated by using the constants $a_1 = 0.05$, $a_2 = -3.3 \times 10^{-4}$, and $a_3 = 9.4 \times 10^{-7}$. The value of a_1 corresponds to a Debye temperature of 34 K, which is close to that for the verdazyl-based complex with the same crystal structure [31]. We calculated the magnetic specific heat assuming the same honeycomb lattice model as for the magnetization susceptibility by using the same parameters and reproduced the observed behavior in the low-temperature region below 10 K, as shown in Fig. 3(c).

C. Numerical analysis on the spin-1/2 distorted honeycomb lattice

The MO calculation results indicate that the three dominant interactions, $J_1/k_B = 7.4$ K, $J_2/k_B = 5.6$ K, and $J_3/k_B = -3.8$ K, lead to the formation an $S = 1/2$ distorted honeycomb lattice. This distorted model can be understood as a J_1-J_2 AF alternating chain connected by ferromagnetic J_3 or a J_1-J_3 AF-ferromagnetic alternating chain connected by AF J_2. To examine the lattice distortion effects on the $S = 1/2$ HAF honeycomb lattice, we simplified the spin lattice such that $J_2 = |J_3|$. We then introduced a distortion ratio $\alpha = J_2/J_1$, which is equivalent to the dimer-like distortion reported in previous numerical studies [10,11], except that J_3 is ferromagnetic. Figures 4(a) and 4(b) show the magnetic susceptibilities and magnetization curves for representative values of α between 0 and 1.0, respectively. The value of J_1 was determined for each α to reproduce the experimental result of χ above 10 K. Thus, the following values were obtained: $J_1/k_B = 4.6$ K ($\alpha = 0.3$), $J_1/k_B = 4.4$ K ($\alpha = 0.5$), $J_1/k_B = 4.3$ K ($\alpha = 0.6$), $J_1/k_B = 4.2$ K ($\alpha = 0.7$), $J_1/k_B = 4.0$ K ($\alpha = 0.8$), and $J_1/k_B = 3.6$ K ($\alpha = 1.0$). The lattice system in the extreme cases, i.e., when $\alpha = 0$ and $\alpha = 1.0$, corresponds to a gapped singlet dimer coupled by J_1 and a gapless uniform honeycomb lattice, respectively. Considering the presence of the energy gap when $\alpha \leqslant 0.6$, clear differences can be observed in the low-temperature regions of χ and the magnetization curve, as shown in Figs. 4(a) and 4(b). The increase in α corresponds to increased two-dimensionality toward the uniform honeycomb lattice when $\alpha = 1.0$, resulting in the disappearance of the energy gap. Accordingly, the magnetization curves exhibit a reduction in the energy gap and approach the experimental gapless behavior with increasing α. Although the experimental results can be well explained with $\alpha = 1.0$, as shown in Figs. 3(a) to 3(c), α dependence is almost indistinguishable when $0.8 < \alpha < 1.0$. These results suggest that the small dimer-like lattice distortion for $0.8 < \alpha < 1.0$ does not affect the intrinsic properties of the present $S = 1/2$ HAF honeycomb lattice. The actual value of α in the present compound should be $0.8 < \alpha < 1.0$. If we assume J_1-J_2 or J_1-J_3 alternating chain, the calculated magnetizations exhibit a gapped behavior [32,33], which is clearly different from the experimental gapless behavior.

Finally, we examined the α dependence of the phase boundaries for the present $S = 1/2$ distorted HAF honeycomb lattice. We predicted the ground-state phase diagram in the α-H plane, as shown in Fig. 5, where the phase boundaries are estimated from the peak structure in the field derivative of the

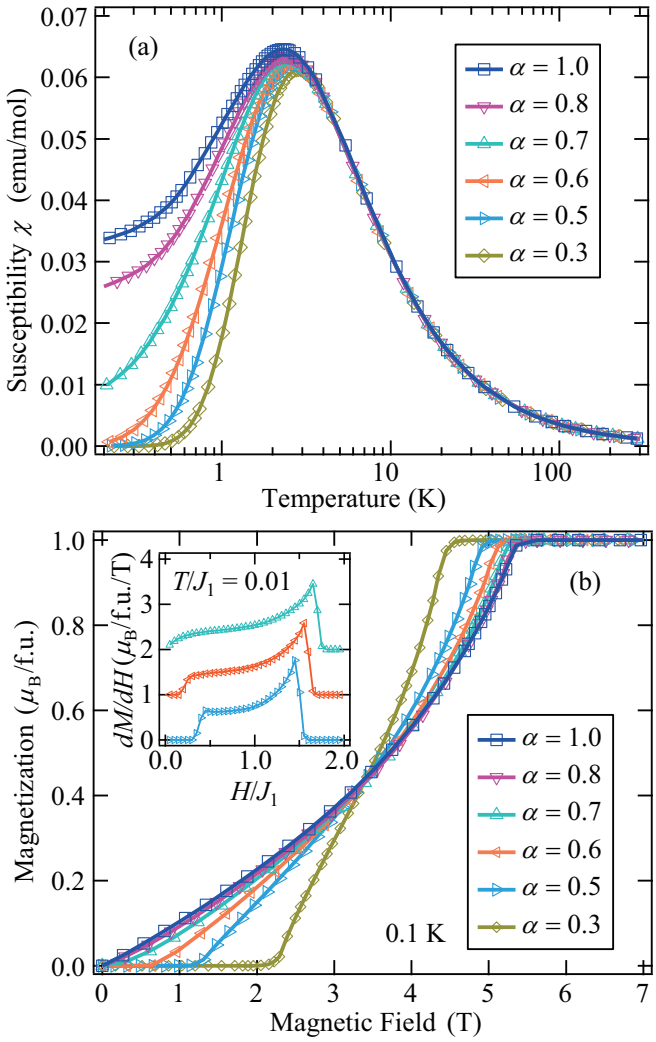

FIG. 4. (a) Calculated magnetic susceptibility and (b) magnetization curves at 0.1 K of the $S = 1/2$ HAF honeycomb lattice assuming $J_2 = |J_3|$ for various values of $\alpha = J_1/J_2$. The inset shows dM/dH at $T/J_1 = 0.01$ near the critical distortion ratio α_c. For clarity, the values of the vertical axes have been shifted up.

magnetization curve at $T/J_1 = 0.01$ for various α, as shown in the inset of Fig. 4(b). The phase diagram can be divided into three regions: a dimer phase, an AF ordered phase (including a canted state), and a fully polarized phase. A QPT from the disordered dimer phase to the AF ordered phase is expected at $\alpha_c \simeq 0.68$. We considered the value of α_c by comparing it to those given in previous theoretical works on similar models. If J_2 and J_3 are equal and AF, the dimer phase region becomes slightly narrower, yielding $\alpha_c \simeq 0.54$ [11]. Conversely, when J_2 and J_3 are equal and ferromagnetic, the dimer phase is stable for most values of α, yielding $|\alpha_c| \simeq 0.93$ [12]. These numerical results suggest that the ferromagnetic correlations in the honeycomb lattice with dimer-like distortion make the AF dimer stable. In the present case, we assumed that J_2 and J_3 are equal and AF and ferromagnetic, respectively. Therefore, the intermediate value of α_c obtained in the present model is consistent with those reported previously.

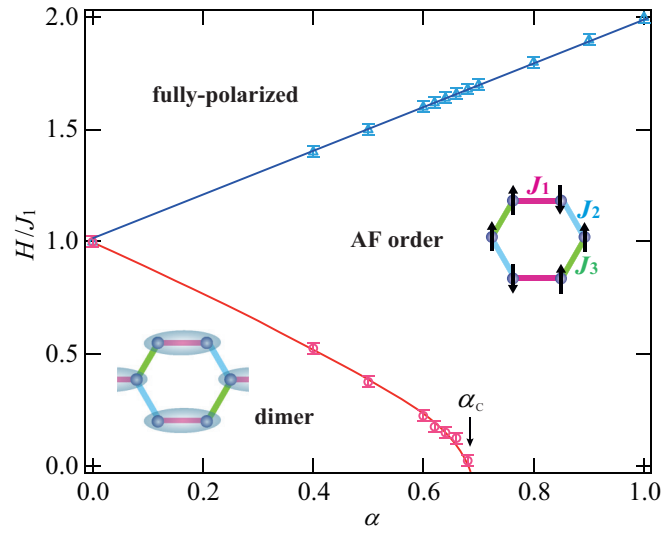

FIG. 5. Ground-state phase diagram of the $S = 1/2$ distorted HAF honeycomb lattice in the α-H plane, characterized by a disordered dimer phase, an AF ordered phase (including a canted state), and a fully polarized phase. The magnetic field H is normalized by J_1. The α_c indicates a QPT. The illustrations show schematic pictures of the singlet dimer and the AF order at zero field.

IV. SUMMARY

We synthesized single crystals of a verdazyl-based complex [Zn(hfac)$_2$][*o*-Py-V-(4-F)$_2$]. *Ab initio* MO calculations indicated three dominant interactions, namely J_1, J_2, and J_3, leading to the formation of an $S = 1/2$ AF honeycomb lattice. The magnetic susceptibility and specific heat indicated the development of AF correlations in the honeycomb plane. The low-temperature magnetization curve exhibited a nonlinear behavior originating from quantum fluctuations in the $S = 1/2$ honeycomb lattice. We explained the magnetic susceptibility, magnetization curve, and magnetic specific heat based on the $S = 1/2$ HAF honeycomb lattice using the QMC method. Further, we examined the lattice distortion effects using a simplified honeycomb lattice with $J_2 = |J_3|$. The dimer-like lattice distortion for $0.8 < \alpha < 1.0$ ($\alpha = J_2/J_1$) did not affect the intrinsic properties of the present $S = 1/2$ HAF honeycomb lattice. Consequently, the actual value of α was expected to be in the range of $0.8 < \alpha < 1.0$ with $J_1/k_B \approx 3.6$–4.0 K. Our numerical study on the α dependence of the magnetic behavior revealed that a QPT occurs from the disordered dimer phase to the AF ordered phase at $\alpha_c \simeq 0.68$.

ACKNOWLEDGMENTS

This research was partly supported by a Grant for Basic Science Research Projects from KAKENHI (Grants No. 17H04850, No. 18H01164, No. 19J01004, and No. 19H04550). A part of this work was performed as the joint-research program of ISSP, the University of Tokyo and the Institute for Molecular Science.

[1] E. Manousakis, Rev. Mod. Phys. **63**, 1 (1991).
[2] X. Du, I. Skachko, F. Duerr, A. Luican, and E. Y. Andrei, Nature **462**, 192 (2009).
[3] A. H. Castro Neto, F. Guinea, N. M. R. Peres, K. S. Novoselov, and A. K. Geim, Rev. Mod. Phys. **81**, 109 (2009).
[4] A. Kitaev, Ann. Phys. (N.Y) **321**, 2 (2006).
[5] Z. Weihong, J. Oitmaa, and C. J. Hamer, Phys. Rev. B **44**, 11869 (1991).
[6] J. Oitmaa, C. J. Hamer, and Z. Weihong, Phys. Rev. B **45**, 9834 (1992).
[7] E. V. Castro, N. M. R. Peres, K. S. D. Beach, and A. W. Sandvik, Phys. Rev. B **73**, 054422 (2006).
[8] U. Löw, Condens. Matter Phys. **12**, 497 (2009).
[9] H. C. Jiang, Z. Y. Weng, and T. Xiang, Phys. Rev. Lett. **101**, 090603 (2008).
[10] K. Takano, Phys. Rev. B **74**, 140402(R) (2006).
[11] W. Li, S.-S. Gong, Y. Zhao, and G. Su, Phys. Rev. B **81**, 184427 (2010).
[12] Y.-Z. Huang, B. Xi, X. Chen, W. Li, Z.-C. Wang, and G. Su, Phys. Rev. E **93**, 062110 (2016).
[13] V. Kataev, A. Möller, U. Löw, W. Jung, N. Schittner, M. Kriener, and A. Freimuth, J. Magn. Magn. Mater. **290**, 310 (2005).
[14] A. A. Tsirlin, O. Janson, and H. Rosner, Phys. Rev. B **82**, 144416 (2010).
[15] Z. Honda, T. Kodama, R. Kikukawa, M. Hagiwara, T. Kida, M. Sakai, T. Fukuda, T. Fujihara, and N. Kamata, J. Phys. Soc. Jpn. **84**, 034601 (2015).
[16] A. Möller, U. Löw, T. Taetz, M. Kriener, G. André, F. Damay, O. Heyer, M. Braden, and J. A. Mydosh, Phys. Rev. B **78**, 024420 (2008).
[17] M. Yehia, E. Vavilova, A. Möller, T. Taetz, U. Löw, R. Kilingeler, V. Kataev, and B. Büchner, Phys. Rev. B **81**, 060414(R) (2010).
[18] S. Okubo, H. Wada, H. Ohta, T. Tomita, M. Fujisawa, T. Sakurai, E. Ohmichi, and H. Kikuchi, J. Phys. Soc. Jpn. **80**, 023705 (2011).
[19] T. Okabe, H. Yamaguchi, S. Kittaka, T. Sakakibara, T. Ono, and Y. Hosokoshi, Phys. Rev. B **95**, 075120 (2017).
[20] H. Yamaguchi, A. Toho, K. Iwase, T. Ono, T. Kawakami, T. Shimokawa, A. Matsuo, and Y. Hosokoshi, J. Phys. Soc. Jpn. **82**, 043713 (2013).
[21] S. Miyamoto, Y. Iwasaki, N. Uemoto, Y. Hosokoshi, H. Fujiwara, S. Shimono, and H. Yamaguchi, Phys. Rev. Mater. **3**, 064410 (2019).
[22] R. Kuhn and H. Trischmann, Monatsh. Chem. **95**, 457 (1964).
[23] G. M. Sheldrick, Acta Crystallogr., Sect. C: Struct. Chem. **C71**, 3 (2015).
[24] H. Yamaguchi, S. Nagata, M. Tada, K. Iwase, T. Ono, S. Nishihara, Y. Hosokoshi, T. Shimokawa, H. Nakano, H. Nojiri, A. Matsuo, K. Kindo, and T. Kawakami, Phys. Rev. B **87**, 125120 (2013).
[25] H. Yamaguchi, Y. Tamekuni, Y. Iwasaki, R. Otsuka, Y. Hosokoshi, T. Kida, and M. Hagiwara, Phys. Rev. B **95**, 235135 (2017).
[26] M. Shoji, K. Koizumi, Y. Kitagawa, T. Kawakami, S. Yamanaka, M. Okumura, and K. Yamaguchi, Chem. Phys. Lett. **432**, 343 (2006).
[27] A. W. Sandvik, Phys. Rev. B **59**, 14157(R) (1999).
[28] A. F. Albuquerque, F. Alet, P. Corboz, P. Dayal, A. Feiguin, L. Gamper, E. Gull, S. Gurtler, A. Honecker, R. Igarashi, M. Korner, A. Kozhevnikov, A. Lauchli, S. R. Manmana, M. Matsumoto, I. P. McCulloch, F. Michel, R. M. Noack, G. Pawlowski, L. Pollet, T. Pruschke, U. Schollwock, S. Todo, S. Trebst, M. Troyer, P. Werner, and S. Wessel, J. Magn. Magn. Mater. **310**, 1187 (2007); see also http://alps.comp-phys.org and http://wistaria.comp-phys.org/alps-looper/.
[29] B. Bauer, L. D. Carr, A. Feiguin, J. Freire, S. Fuchs, L. Gamper, J. Gukelberger, E. Gull, S. Guertler, A. Hehn, R. Igarashi, S. V. Isakov, D. Koop, P. N. Ma, P. Mates, H. Matsuo, O. Parcollet, G. Pawlowski, J. D. Picon, L. Pollet, E. Santos, V. W. Scarola, U. Schollwöck, C. Silva, B. Surer, S. Todo, S. Trebst, M. Troyer, M. L. Wall, P. Werner, and S. Wessel, J. Stat. Mech.: Theory Exp., (2011) P05001.
[30] H. Yamaguchi, K. Iwase, T. Ono, T. Shimokawa, H. Nakano, Y. Shimura, N. Kase, S. Kittaka, T. Sakakibara, T. Kawakami, and Y. Hosokoshi, Phys. Rev. Lett. **110**, 157205 (2013).
[31] H. Yamaguchi, Y. Shinpuku, T. Shimokawa, K. Iwase, T. Ono, Y. Kono, S. Kittaka, T. Sakakibara, and Y. Hosokoshi, Phys. Rev. B **91**, 085117 (2015).
[32] S. Watanabe and H. Yokoyama, J. Phys. Soc. Jpn. **68**, 2073 (1999).
[33] Y. Iwasaki, Y. Sasaki, Y. Hosokoshi, A. Matsuo, K. Kindo, and H. Yamaguchi, J. Phys. Soc. Jpn. **88**, 044709 (2019).